Nanoscale

Tailored Synthesis of Molecularly-Thin Platinum Nanosheets Using Designed 2D Surfactant Solids

Journal:	*Nanoscale*
Manuscript ID	NR-ART-04-2022-001807.R1
Article Type:	Paper
Date Submitted by the Author:	31-May-2022
Complete List of Authors:	Yamamoto, Eisuke; Nagoya University, Institute of Materials and Systems for Sustainability Suzuki, Akiko; Nagoya University, Institute of Materials and Systems for Sustainability Kobayashi, Makoto; Nagoya University Ecotopia Science Institute, Furo-cho, Chikusa-ku Osada, Minoru ; Nagoya University

ARTICLE

Tailored Synthesis of Molecularly-Thin Platinum Nanosheets Using Designed 2D Surfactant Solids

Received 00th January 20xx,
Accepted 00th January 20xx

DOI: 10.1039/x0xx00000x

Eisuke Yamamoto[a,b]*, Akiko Suzuki[a], Makoto Kobayashi[a] and Minoru Osada[a,c*]

The assembly of the surfactants has been utilized as the unique templates for metal nanosheets. However, current strategies for metal nanosheets have mainly focused on the liquid-phase surfactant assembly. Here, we found the solid-state surfactants as designable crystals suitable for nanostructural control, and proposed a novel synthetic route for molecularly-thin Pt metal nanosheets using solid surfactant crystals as a precursor. The 2D surfactant crystals containing planarly arranged Pt complexes were prepared, and the subsequent UV-ozone treatment and reduction process allowed us to obtain the Pt metal nanosheets. The Pt metal nanosheets had a distinct morphology with a various thickness (from 1.5 nm to 3.0 nm), inherent from those of 2D surfactant crystals.

Introduction

The controlled synthesis of nanomaterials into desired architectures is at the heart of nanomaterials research.[1–4] Nanostructured metals are one of the essential targets in this regard; nanostructured metals with different shapes and sizes often exhibit unique functionalities, different from their bulk counterparts. The surfactants play a key role for the design of morphology and structure of nanostructured metals, owing to their usefulness in versatile conditions, such as growth controls and increasing dispersibility.[5] In particular, the surfactants can be assembled into the various superstructures, including micelles[6], liquid crystals[7,8], and self-assembled monolayer[9], offering the nanoscale design via templating the assembled structures. Therefore, the surfactant templating methods are fundamental techniques for nanostructured metals, despite the demanding control on the superstructure. Further development of the surfactant assembly depends on finding a novel approach that enables the precise design of nanostructures with desired functionalities.[10]

Such an issue is particularly important for designing 2D metal nanosheets.[11,12]2D metal nanosheets have attracted great attention because they exhibited a drastic change in physicochemical properties owing to 2D confinement effects.[13] In particular, due to their unique 2D morphology with exceptionally large exposed surface area, 2D nanosheets can significantly enhance surface reactions, redox processes, and charge separations. The synthetic approach using the surfactant assembly is one of the solutions for generating 2D metal nanosheets.[14–17] Typically, the concentrated surfactant micelles solutions form lamellar liquid crystals possessing the 2D nano-space; the use of interlayer nano-space of the lamellar liquid crystals has been well documented as an ideal template for the confined growth of the 2D metal nanosheets. However, control of the thickness and morphology of the metal nanosheets still remains a real challenge. Due to their fragile nature, lamellar liquid crystals usually lack a strong confinement force to regulate the 2D anisotropic growth; metal atoms tend to form 3D structures. In addition, the structure of the lamellar liquid crystals was easily changed by various factors, including temperature, concentration, and precursor amount.[18–20] Therefore, the synthesis of the metal nanosheets using the surfactant assembly faces difficulty in the systematic design.

The previous strategies using the surfactant assembly have only focused on the liquid-phase surfactants; nevertheless, it is known that the surfactants form unique solid phases with a crystalline state under the Krafft point.[21,22] The crystalline solid phase (*Lc* phase) surfactants have a lamellar structure with densely arranged counter ions in the interlayer space and the distinct morphology reflecting the crystal habit. Interestingly, the structure and morphology of surfactant crystals have the potential for design depending on the component's structure and composition, different from liquid crystals.[21,23–25] Therefore, templating the solid surfactant crystals with distinct thickness and morphology will allow the precise design of the metal nanosheets, offering the potential for a novel technique for nanoarchitectonics of metal nanosheets. However, to the best of our knowledge, the surfactant assembly with the solid crystalline phase has never been used for the designed synthesis of nanostructured materials.

Here, we report a new concept for the designed synthesis of molecularly-thin metal nanosheets using solid-state surfactant crystals. As typical metal nanosheets, Pt metal nanosheets were synthesized because they are potential candidates for future nanosheets devices and catalysts.[26] We synthesized the surfactant

[a] *Department of Materials Chemistry & Institute of Materials and Systems for Sustainability (IMaSS), Nagoya University, Nagoya 464-8601, Japan.*
[b] *Precursory Research for Embryonic Science and Technology (PRESTO), Japan Science and Technology Agency (JST), Saitama 332-0012, Japan.*
[c] *International Center for Materials Nanoarchitectonics (WPI-MANA), National Institute for Materials Science (NIMS), Tsukuba 305-0044, Japan.*
Electronic Supplementary Information (ESI) available. See DOI: 10.1039/x0xx00000x

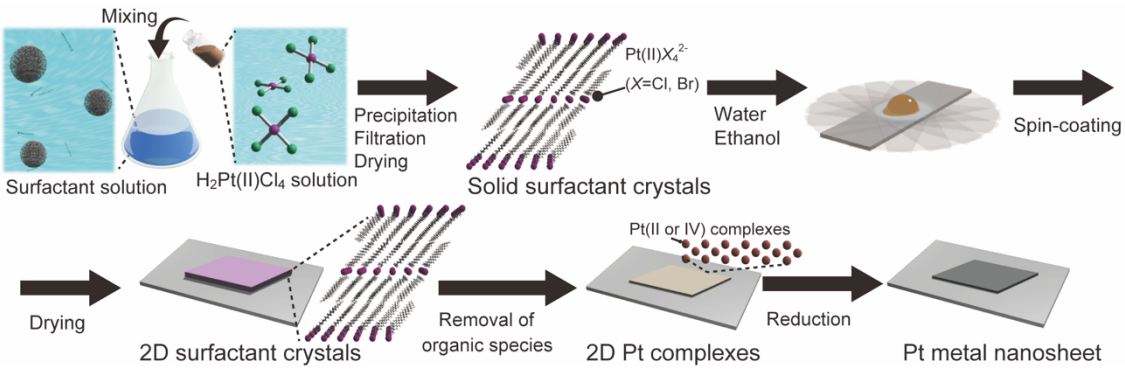

Fig. 1 Schematic process of the molecularly-thin Pt metal nanosheets using surfactant crystals.

crystals with planarly arranged Pt complexes as a precursor and designed the morphology and thickness of the 2D surfactant crystals via the recrystallization process. Then, the 2D surfactant crystals were treated with UV-ozone and reduced by H_2(5%)/Ar. These processes lead to the synthesis of molecularly-thin Pt metal nanosheets, inherent from the thickness and morphology of 2D surfactant crystals (Fig.1). We have also succeeded in structural analysis of surfactant crystals and found that there is a clear correlation between the thickness and morphology of 2D surfactant crystals and the resulting metal nanosheets. This method is potentially useful for precisely design of the molecularly-thin metal nanosheets with distinct morphology and thickness.

Results and discussion

Preparation of solid surfactant crystals containing Pt complexes. The surfactant crystals were prepared as powder by mixing the aqueous solution of cetyltrimethylammonium bromide (CTAB) and $H_2Pt(II)Cl_4$. For evaluation of the crystal structure, the single crystal X-ray diffraction measurement was conducted. The single crystal of surfactant with a distinct rhombus morphology was prepared by adding water as a poor solvent to the mixed solvent of N-methylformamide and 2-propanol dissolving the powder surfactant crystal at 298 K (Fig. 2 (a)). The structure was determined to be in a triclinic system (*P*-1) with a composition of $[(C_{16}H_{33})N(CH_3)_3]_2[PtBr_{0.4}Cl_{3.6}]$ and lattice constants of a = 7.59250(10) Å, b = 8.14060(10) Å, c = 20.0035(2) Å, α = 88.8910(10) °, β = 80.8020(10)°, and γ = 66.2290(10)°. Pt ions are coordinated by Br and Cl ions, which occupy two sites disorderly, and have a square-planar geometry with a C_{2h} symmetry. The alkylammonium cation are aligned orderly in *ab*-plane resulting in the formation of the layered structure, which indicates the formation of the solid-state crystalline phase. In addition, the Pt complexes are arranged planarly as the interlayer counter ions. The distance between two Pt complexes at different interlayer spaces is approximately 2.0 nm (Fig. 2(b)). The condition for crystal structure refinement is shown in the ESI.

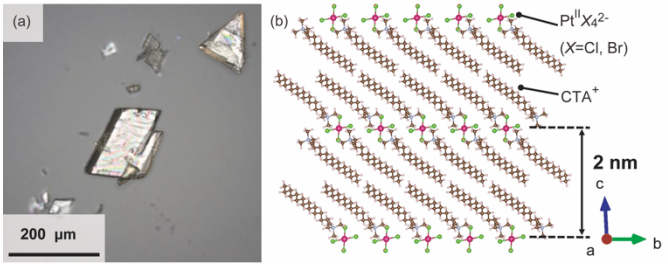

Fig. 2 (a) Appearance of the single crystalline surfactants with Pt complexes, and (b) the refined crystal structure.[27]

Synthesis of Pt metal nanosheets. The 2D surfactant crystals were prepared on a Si substrate by evaporating the mixed solution of water and ethanol dissolving the surfactants crystals. For the formation of the 2D surfactant crystals, control of the evaporation process was essential. The simple drying of the liquid droplet is not practical for 2D growth of the surfactant crystals because it led to the formation of bulk state crystals (Fig.S1 (a) of the ESI). We found that thin 2D surfactant crystals could be obtained under the centrifugal force via spin coating. With the continuous loss of the surfactant solutions via spin coating, the fluid layer becomes thinner and flat; 2D surfactant crystals can form in such a thin fluid layer. Finding the proper conditions, the rotation speed of the spin coating was varied from 1500 rpm to 5000 rpm. At the slow rotation speed of 1500 rpm, the large-sized bulk crystals were mainly obtained (Fig. S1 (b) of the ESI), while a homogeneous non-crystalline film was formed by applying over 5000 rpm (Fig. S1 (d) of the ESI). The optimal condition was found to be 2000 ~ 4000 rpm, where the controlled synthesis of the 2D surfactant crystals was achieved (Fig.S1(c), (d), and (e) of the ESI). Almost all the 2D surfactant crystals showed a rhombus morphology reflecting the crystal structure. The obtained 2D surfactant crystals have wide thickness distribution under any conditions. For example, the 2D surfactant crystals with approximately 60 nm in mean thickness (in the range from 20 nm to 90 nm) were formed at the 2000 rpm condition. Although they have a wide distribution in the thickness range, the mean thickness of the 2D nanosheets tends to decrease slightly as increasing the rotation speed of the spin coating.

As a typical example, 2D surfactant crystals were prepared via 2000 rpm coating, and the thickness of the sheet was monitored at each step. As seen from the AFM image, the thickness of the 2D surfactant crystal was evaluated as 49 nm, which corresponds to 24 layers of the surfactant bilayer considering the crystal structure (Fig. 3(a) and (d)). The XRD and XPS measurements and Raman spectroscopy analysis were conducted to confirm the crystal structure. Fig. S2 (a) of the ESI shows the XRD pattern of the 2D surfactant crystals. The XRD pattern showed clear peaks at 4.5, 9.0, and 13.5 ° assigned to 001, 002 and 003 reflections of the surfactant crystals, respectively. The Raman spectrum showed the retention of the surfactant as shown by broad peaks derived from the stretching of C-H groups in

the alkyl chain (CH_2 and CH_3) at 2900 cm^{-1} (Fig. S2 (c) of the ESI). In addition, XPS spectrum of the 2D surfactant crystals showed clear peaks at 75.2 eV and 72.0 eV derived from $Pt^{2+}4f_{5/2}$ and $Pt^{2+}4f_{7/2}$ (Fig. 1(g)). Although the peaks derived from Br3d (68 eV) are unclear, a peak derived from $Cl2p_{3/2}$ was clearly observed at 198 eV, indicating the retention as the Pt halides (Fig. S2 (e) of the ESI). These results indicate the formation of the 2D surfactant crystals with the same structure as the single crystal bulk.

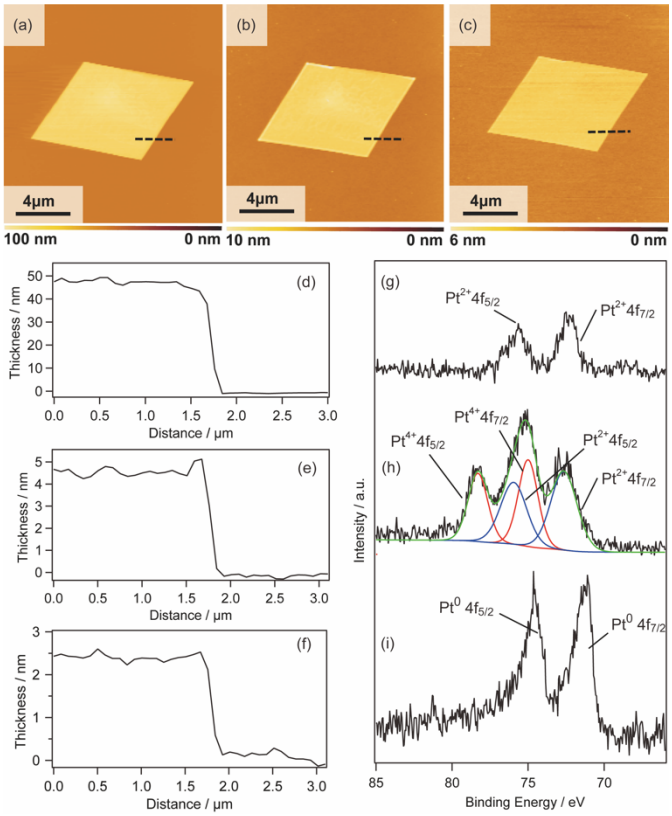

Fig. 3 AFM images, height profiles, and XPS spectra of the 2D sheets: (a), (d), and (g) 2D surfactant crystals, (b), (e), and (f) 2D Pt complexes, and (c), (f) and (i) Pt metal nanosheets.

The Pt metal nanosheets were synthesized via UV-ozone treatment of 2D surfactant crystals and subsequent reduction process under a H_2 (5%)/Ar flow. We characterized the samples at each step for clarifying the effects of UV-ozone treatment and reduction process under a H_2 (5%)/Ar flow. Firstly, the 2D surfactant crystals were treated with UV-ozone to selectively remove the organic species. The other processes, such as calcination at mild conditions, lead to the collapse of the 2D structure (Fig.S3 of the ESI). A key for maintaining the 2D morphology is the intermediate UV-ozone treatment; the direct reduction of the 2D surfactant crystals leads to the formation of discrete large-sized Pt nanoparticles (Fig. S4 of the ESI). The morphological change by UV-ozone treatment on the 2D Pt complexes was observed by AFM (Fig. 3(b)). The thickness of the 2D Pt complexes was drastically decreased from 49 nm to 4.7 nm with retaining the surface roughness and lateral size. In addition, the composition and structure of the 2D Pt complexes were evaluated by Raman spectroscopy analysis and XRD measurement. No clear peak attributed to stretching of C-H groups (2900 cm^{-1}) was observed in the Raman spectrum (Fig. S2 (d) in the ESI), indicating the removal of CTA^+. The removal of the surfactant corresponds to the fact that the XRD pattern did not show the peaks derived from the ordered structure (Fig. S2(b) in the ESI). Notably, the Pt species were partially oxidized via UV-ozone treatment as detected by the XPS measurement. The peaks derived from $Pt^{2+}4f_{5/2}$, $Pt^{2+}4f_{7/2}$, $Pt^{4+}4f_{7/2}$, and $Pt^{4+}4f_{5/2}$ were observed, and the ratio of Pt^{2+}/Pt^{4+} was roughly calculated to be 1.2 (Fig. 3(h)). The mixture of Pt oxide and halide should be formed after UV-ozone treatment considering the broad peaks of $Cl2p_{3/2}$. From these results, it was confirmed that the 2D nanosheets composed of the Pt complex without organic species were formed after UV-ozone treatment.

The molecularly-thin Pt metal nanosheets were synthesized by reducing the 2D Pt complexes under a H_2 (5%)/Ar flow. For optimizing the conditions, the reductions were carried out at 120, 200, and 300 °C. The reduction condition of the Pt complex is an important factor, and discrete nanoparticles assemblies were formed at 200 and 300 °C (Fig. S5 (a) and (b) of the ESI). We succeeded in maintaining a nanosheet structure through reduction at 120 °C (Fig. 3(c)). Note that the complete reduction of the Pt species required a long-time treatment because Pt^{2+} species partially remained when the nanosheets were reduced for 5 h (Fig. S5 (c) and (d) of the ESI). After reduction treatment for 20 h, the asymmetrical peaks attributed to $Pt^0 4f_{5/2}$ and $Pt^0 4f_{7/2}$ were mainly obtained, indicating the formation of Pt metal nanosheets (Fig. 3(i)). AFM image of the sample after hydrogen reduction at 120°C for 20 hours showed an articulate decrease in thickness of the nanosheet from 4.7 to 2.3 nm (Fig. 3 (e)). The surface roughness of the nanosheets is almost the same as the substrate. In addition, the high-resolution AFM observation showed that the surface of the nanosheet was very smooth, although nanoparticles were observed (Fig. S6 (a) and (b) of the ESI). The theoretical thickness calculated by the amount of the Pt species in the 2D surfactant crystals with 49 nm thickness should be approximately 0.7 nm by considering the 21.45 gcm^{-3} as the density. It is known that AFM observation of 2D materials often overestimates the thickness due to adsorbed molecules on the nanosheet surface and water adlayers on the substrate. For example, the thickness of the monolayer graphene was evaluated as 0.7 nm in spite of 0.4 nm in the real thickness because of the water adlayers.[28] However, the measured 2.3 nm thickness is too different from the theoretical value (0.7 nm) even if there were adsorbates. Therefore, there should be some voids in the nanosheet structure, maybe due to the interparticle space of polycrystalline continuous Pt nanosheets. Although the obtained nanosheets should be composed of polycrystalline Pt nanoparticles, such polycrystalline nanosheets also tend to exhibit unique properties different from nanoparticles and bulks.[29] The obtained molecularly-thin Pt metal nanosheets with large lateral size and distinct rhombus morphology should be useful for their application and fundamental investigation of properties.

The synthesis of Pt metal nanosheets with varied thicknesses and morphologies. We also investigated the versatility of this method using different substrates, such as MgO and Al_2O_3. The 2D surfactant crystals were formed successfully regardless of the kinds of substrates, and metal nanosheets should be formed via reduction after UV-ozone treatment. All obtained nanosheets were appropriately 2 nm in thickness, as shown by AFM images (Fig. S7 (a), (b), (c), and (d) in the ESI). Therefore, this method has potential for

the synthesis of Pt metal nanosheets on various substrates as long as the substrate has stability against the UV-ozone treatment and the hydrogen reduction at 120 °C.

In addition, the morphologies of the metal nanosheets synthesized using different precursors were investigated. As typical examples, Pt metal nanosheets were also synthesized using $K_2Pt(IV)Cl_6$ as a metal complex precursor (Fig. 4 (a) and (b)) or CTAC as a surfactant precursor (Fig. S7 (e) and (f) in the ESI). When the metal nanosheets were synthesized using CTAC, the morphology of the nanosheets was not changed from the rhombus type (Fig. S7 (g) and (h) in the ESI). In contrast, interestingly, the use of $K_2Pt(IV)Cl_6$ lead to the morphological change of nanosheet into hexagonal, probably reflecting the crystal habit of the surfactant crystals (Fig. 4). Although the crystals structure of the surfactant is under investigation, there should be the possibility on the control of the morphology through the choice of the precursors. As considering the previous molecularly-thin Pt nanosheets have undefined morphology, this method may open the platform for designing the morphology of the molecularly-thin Pt nanosheets.

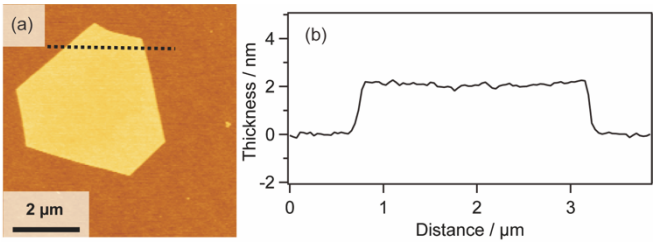

Fig. 4 (a) AFM image and (b) height profile of the metal nanosheets synthesized using $K_2Pt(IV)Cl_6$ as a metal complex precursor.

Furthermore, it is known that the thickness of metal nanosheets has a significant impact on their structures and properties, and the sub-nm level thickness control is an important issue.[13] Although many methods have been proposed to synthesize Pt metal nanosheets,[15,29–39] the thickness and morphology control still remain challenging issues. In order to control the thickness of the molecularly-thin nanosheets, we investigated the relationship of thickness between the 2D surfactant crystals and Pt metal nanosheets. The thickness of the nanosheets was monitored at each step using 4 samples with different thicknesses (Fig. S8 in the ESI). Table 1 shows the thickness variation for each of the four nanosheets. In all cases, the thicknesses were decreased into 10 % when the 2D surfactant crystals were changed into 2D Pt complexes. Subsequently, the thickness was decreased into 7-8 % when the 2D complexes were reduced to Pt metal nanosheets. Considering the relationship, the thickness of the Pt metal nanosheets could be varied quite finely via thickness control of the 2D surfactant crystals. This method should have the potential for sub-nm thickness control of Pt metal nanosheets. In addition, this method may also have the potential for increasing the lateral size of nanosheets via optimization of the 2D surfactant synthesis condition. The Pt metal nanosheets with a large lateral size (15 μm) were also synthesized using a coincidently formed large 2D surfactant as a precursor (Fig. S9 in the ESI). Although the synthetic condition for 2D surfactant with a large lateral size is not optimized, such large-sized nanosheets have been preferred to investigate the fundamental property of the metal nanosheets.

Table 1 Thicknesses of the nanosheets at each process

Sheet No.	2D surfactant crystal	2D Pt complex	Pt metal nanosheet
1	48 nm	4.5 nm	3.0 nm
2	30 nm	3.0 nm	2.3 nm
3	29 nm	2.8 nm	2.2 nm
4	20 nm	2.0 nm	1.5 nm

Stability of the Pt nanosheets. We investigate their stability against solvents, which is essential for their practical use. The obtained nanosheets were immersed for 1 day in water or ethanol and investigated their structural changes. However, the obtained Pt metal nanosheets were unstable in both solvents. For example, when the nanosheet with a thickness of 2.0 nm was immersed in water for 1 day, the thickness increased to 3 nm (Fig. 5 (a) and (c)). The increase in the thickness was caused via morphological change of the nanosheets component, which means the formation of large-sized nanoparticles as shown by high-resolution AFM image (Fig. 5 (b)). The surface roughness (Ra) of the nanosheets was increased from 140 pm to 490 pm, also supporting the formation of the nanoparticle.

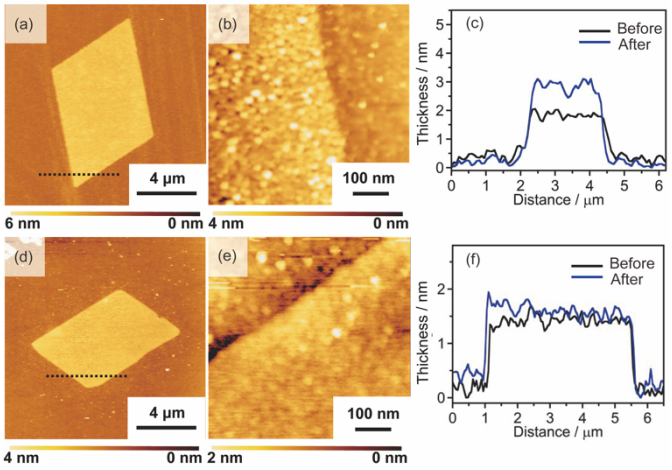

Fig. 5 The AFM images and height profiles of Pt metal nanosheets after immersing those in water for 1 day: (a), (b) and (c) the Pt metal nanosheet before calcination, and (d), (e), and (f) the Pt metal nanosheet after calcination.

We found that the calcination of Pt nanosheets at 800 °C suppresses the formation of the large-sized nanoparticles. The calcined nanosheets exhibited high stability against solvents, and no morphological change was observed via immersing the nanosheets into the water for 1 day (Fig. 5 (a), (b), and (c)). Therefore, we evaluated the structure of the Pt metal nanosheets after calcination. In the calcination process, the thickness of the nanosheets was slightly changed from 2.3 nm into 2.0 nm while keeping the morphology (Fig. S10 (a) in the ESI). The decrease in the thickness should be derived from the removal of adsorbed molecules or

shrinkage of the void volume. The surface of the nanosheets was very flat, and no particle was observed (Fig. S11 (b) in the ESI). The chemical states of the nanosheets were not changed as shown by the XPS spectrum showed only peaks derived from metallic Pt species (Fig. S10 (c) in the ESI). The in-plane XRD measurement probably showed very weak peaks assigned to Pt with an fcc structure (Fig. S10 (d) in the ESI). Although a complete understanding on the structure of the obtained nanosheets awaits further studies, this process may be effective for obtaining stable metal nanosheets with precisely controlled thickness.

Conclusions

We have demonstrated a synthetic approach of molecularly-thin 2D Pt metal nanosheets using solid surfactant crystals as a precursor. This method requires three steps. i) Preparation of surfactant crystals containing planarly arranged Pt complex and their 2D anisotropic growth on the target substrate. ii) Formation of 2D Pt complex through selective removal of alkylammonium cation via UV-ozone treatment. iii) The reduction of the 2D Pt complex via a mild condition under H_2 (5%)/Ar flow. This method has potential for various substrates which have stability against UV-ozone treatment and hydrogen gas treatment under 120 °C. In addition, the thickness of the nanosheets can be controlled from 1.5 nm to 3.0 nm depending on the thickness of the 2D surfactant crystals, offering the potential for a novel method for precisely controlled metal nanosheets. Although the obtained Pt metal nanosheets were unstable against the solvents, calcination led to the drastic improvement of the stability. This method is potentially useful for precisely designing molecularly-thin metal nanosheets with distinct morphology and thickness.

Experimental

Materials. All the materials were used without further purification. Hexadecyltrimethylammonium bromide (CTAB), Hexadecyltrimethylammonium chrolide (CTAC), ethanol and 2-propanol (>99.7 %) were purchased from Kishida Chemical Co., Ltd. Potassium tetrachloroplatinate(II) (99.9 %), potassium hexachloroplatinate(IV) (99.9 %), N-methylformamide (NMF) (>99.0 %) were purchased from FUJIFILM Wako Pure Chemical Co., Ltd.

Preparation of lamellar crystals containing Pt complexes. $K_2Pt(II)Cl_4$(0.5 g) was dissolved in 10 mL of water, and 10 mL of water containing CTAB (0.878 g) was added into the mixture at 60 °C. The precipitates were filtered after standing the solution 24 h, and the obtained precipitates were washed by water. The collected slurry was dried at room temperature to form surfactant crystals. The surfactant crystals were also prepared using $K_2Pt(IV)Cl_6$ or CTAC. The formation of the surfactant crystals prepared with $K_2Pt(IV)Cl_6$ was confirmed by XANES and XRD measurements, Raman spectroscopic analysis and SEM observation (Fig. S11 in the ESI).

Synthesis of molecularly-thin Pt nanosheets. The obtained lamellar crystals (0.5 mg) were dissolved in the mixture of ethanol (2 mL) and water (1 mL). Then, the obtained dispersion was dropped on the different substrates including Si, MgO and Al_2O_3. Subsequently, the spin coating was conducted twice with 1500, 2000, 3000, 4000 or 5000 rpm. The 2D surfactant crystals were formed after drying substrates carefully. Then, the 2D surfactant crystals were treated by UV-Ozone for 4 days to remove the organic species selectively. Finally, the sample was reduced under H_2 gas flow condition (H_2(5%)/Ar, 50 mLmin^{-1}) at 120 °C for 20 h.

X-ray crystallography. Single crystals of surfactants were prepared by adding water as a poor solvent to the mixed solvent of NMF and 2-propanol dissolving surfactant with Pt complex at 298 K. A colorless platelet single crystal with a dimension of 0.10 × 0.07 × 0.02 mm^3 was picked up, and was affixed to a Mitegen mount with a drop of Paratone-N oil. It set to a goniometer of a single-crystal X-ray diffractometer (Rigaku, Rigaku XtaLAB). X-ray diffraction data of the single crystal were collected using MoKα radiation at 151 K with multi-layer mirrors and a hybrid pixel array detector (Rigaku, HyPix-6000 area detector). Unit cell refinement and absorption collection were performed by the program CrysAlisPro 1.171.40.82a (Rigaku Oxford Diffraction). The crystal structure was solved by direct methods using the SHELXT program[40] and structure parameters were refined by full-matrix least-squares on F^2 using the SHELXL2018 program.[41] All calculations were conducted using the WinGX software package.[42] Crystal data, data collection and structure refinement details are summarized in Table S1, and a moiety of the compound is presented in Fig. S12 in the ESI. Crystallographic data reported in this manuscript have been deposited with Cambridge Crystallographic Data Centre as supplementary publication no. CCDC-2161128.

Characterization. AFM images were obtained on MFP3D-origin (Oxford Instruments). Scanning electron microscope (SEM) images were observed by a JEOL JSM-7610fplus operating at 5 kV. Powder X-ray diffraction (XRD) patterns were observed by a RIGAKU Smart Lab operating at 45kV and 200 mV. The crystal structure was illustrated with VESTA software package.[27] Confocal laser microscope images were obtained by an Olympus OLS4000. CHN elemental analyses were conducted by a micro corder (J-science group JM10). Thermogravimetry (TG) curves were obtained on a HITACHI STA7200 under air flow at a heating rate of 10 °C min^{-1} up to 900 °C. Raman spectra were obtained by a HORIBA-Jobin-Yvon LabRAM HR800. XPS spectra were obtained by a Fisher Scientific ESCALAB 250Xi. The X-ray absorption find structure (XAFS) data was collected at BL01B1 beamline in SPring-8.

Author Contributions

The manuscript was written through the contributions of all authors. E. Y. contributed to make the concept of the synthesis and preparation of the manuscript. E.Y. and A. S. experimented with the synthesis of nanosheets. M. K. performed the single crystalline X-ray analysis, evaluation on the composition of surfactant crystals and discussed the data. M. O. discussed the data and revised essential content in the manuscript.

Conflicts of interest

There are no conflicts to declare.

Acknowledgements

This work was supported by the Grant-in-Aid for Scientific Research for young scientists (19K15656), JSPS, PRESTO (JPMJPR19TA), JST, the Grant-in-Aid for Scientific Research (21H05015, 21H04617, 19K22104), JSPS, and A-STEP, JST, DEJI²MA, MEXT, and the joint usage / research program of IMaSS, Nagoya University, Japan. In addition, we thank Prof. H. Kato (Tohoku University), Dr. I. Hayashi (Nagoya University), Dr. Y. Taniguchi (Oxford instruments) and Mr. D. Kurimoto (Nagoya University) for the experimental assistance.

Notes and references

1. C. Zhu, D. Du, A. Eychmüller and Y. Lin, *Chem. Rev.*, 2015, **115**, 8896–8943.

2. G. V. Hartland, *Chem. Rev.*, 2011, **111**, 3858–3887.

3. Q. Shi, C. Zhu, D. Du and Y. Lin, *Chem. Soc. Rev.*, 2019, **48**, 3181–3192.

4. M. Zahmakırana and S. Özkar, *Nanoscale.*, 2011, **3**, 3462–3481.

5. B. Wu and N. Zheng, *Nano Today*, 2013, **8**, 168–197.

6. T. K. Sau and A. L. Rogach, *Adv. Mater.*, 2010, **22**, 1781–1804.

7. K. Ariga, A. Vinu, Y. Yamauchi, Q. Ji and J. P. Hill, *Bull. Chem. Soc. Jpn.*, 2012, **85**, 1–32.

8. Y. Yusuke, T. Azusa, K. Masaki, S. Makoto, O. Tetsu and K. Kazuyuki, *Chem. Mater.*, 2008, **20**, 1004–1011.

9. N. K. Chaki and K. Vijayamohanan, *Biosens. Bioelectron.*, 2002, **17**, 1–12.

10. K. Ariga X. Hu, S. Mandal and J. P. Hill, *Nanoscale*, 2010, **2**, 198–214.

11. R. Dong, T. Zhang and X. Feng, *Chem. Rev.*, 2018, **118**, 6189–6235.

12. F. Nosheen, N. Wasfi, S. Aslam, T. Anwar, S. Hussain, N. Hussain, S. N. Shah, N. Shaheen, A. Ashraf, Y. Zhu, H. Wang, J. Ma, Z. Zhang and W. Hu, *Nanoscale*, 2020, **12**, 4219–4237.

13. L. Wang, Z. Zeng, W. Gao, T. Maxson, D. Raciti, M. Giroux, X. Pan, C. Wang and J. Greeley, *Science*, 2019, **363**, 870–874.

14. J. Niu, D. Wang, H. Qin, X. Xiong, P. Tan, Y. Li, R. Liu, X. Lu, J. Wu, T. Zhang, W. Ni and J. Jin, *Nat. Commun.*, 2014, **5**, 3313.

15. H. Kawasaki, M. Uota, T. Yoshimura, D. Fujikawa, G. Sakai, M. Annaka and T. Kijima, *Langmuir*, 2005, **21**, 11468–11473.

16. H. L. Qin, D. Wang, Z. L. Huang, D. M. Wu, Z. C. Zeng, B. Ren, K. Xu and J. Jin, *J. Am. Chem. Soc.*, 2013, **135**, 12544–12547.

17. B. Jiang, Y. Guo, J. Kim, A. E. Whitten, K. Wood, K. Kani, A. E. Rowan, J. Henzie and Y. Yamauchi, *J. Am. Chem. Soc.*, 2018, **140**, 12434–12441.

18. P. B. Warren and M. Buchanan, *Curr. Opin. Colloid In.*, 2001, **6**, 287–293.

19. M. G. Berni, C. J. Lawrence and D. Machin, *Adv. Colloid Interfac.*, 2002, **98**, 217–243.

20. A. Khan, *Curr. Opin. Colloid In.*, 1996, **1**, 614–623.

21. R. M. Miller, J. T. Cabral, E. S. J. Robles, N. J. Brooks and O. Ces, *Crystengcomm*, 2018, **20**, 6834–6843.

22. T. Lee, K. Yeh, J. You, Y. Fan, Y. Cheng and D. Pratama, *ACS Omega*, 2020, **5**, 1068–1079.

23. V. M. Coiro and F. Mazza, *Acta Crystallog. Sect. C*, 1989, **45**, 1132–1136.

24. V. M. Coiro and F. Mazza, *Acta Crystallog. Sect. C*, 1991, **47**, 1169–1173.

25. L. A. Smith, R. B. Hammond, K. J. Roberts, D. Machin and G. McLeod, *J. Mol. Struct.*, 2000, **554**, 173–182.

26. W. Sugimoto and D. Takimoto, *Chem. Lett.*, 2021, **50**, 1304–1312.

27. K. Momma and F. Izumi, *J. Appl. Crystallogr.*, 2011, **44**, 1272–1276.

28. X. Ke, C. Peigen and H. J. R., *Science*, 2010, **329**, 1188–1191.

29. A. Funatsu, H. Tateishi, K. Hatakeyama, Y. Fukunaga, T. Taniguchi, M. Koinuma, H. Matsuura and Y. Matsumoto, *Chem. Commun.*, 2014, **50**, 8503–8506.

30. M. Sodeno, S. Kato, H. Nanao and M. Shirai, *Catal. Today*, 2021, **375**, 48–55.

31. M. Shirai, *Chem. Rec.*, 2019, **19**, 1263–1271.

32. M. Chhetri, M. Rana, B. Loukya, P. K. Patil, R. Datta and U. K. Gautam, *Adv. Mater.*, 2015, **27**, 4430–4437.

33. M. Shirai, K. Igeta and M. Arai, *Chem. Commun.*, 2000, 623–624.

34. Z. Fan, Y. Zhu, X. Huang, Y. Han, Q. Wang, Q. Liu, Y. Huang, C. L. Gan and H. Zhang, *Angew. Chem. Int. Ed.*, 2015, **54**, 5672–5676.

35. F. Saleem, Z. Zhang, B. Xu, X. Xu, P. He and X. Wang, *J. Am. Chem. Soc.*, 2013, **135**, 18304–18307.

36. X. Bao, Y. Gong, X. Zheng, J. Chen, S. Mao and Y. Wang, *J. Energy Chem.*, 2020, **51**, 272–279.

37. S. Takenaka, S. Miyake, S. Uwai, H. Matsune and M. Kishida, *J. Phys. Chem. C*, 2015, **119**, 12445–12454.

38. S. Takenaka, H. Arita, K. Sugiyama and K. Nakatani, *Chem. Lett.*, 2018, **47**, 975–978.

39. F. Saleem, B. Xu, B. Ni, H. Liu, F. Nosheen, H. Li and X. Wang, *Adv. Mater.*, 2015, **27**, 2013–2018.

40. G. M. Sheldrick, *Acta Crystallogr. Sect. C Struct. Chem.*, 2015, **71**, 3–8.

41. G. M. Sheldrick, *Acta Crystallogr. Sect. Found. Adv.*, 2015, **71**, 3–8.

42. L. J. Farrugia, *J. Appl. Crystallogr.*, 2012, **45**, 849–854.